### Title

Defective mitochondrial disulfide relay system, altered mitochondrial morphology and function in Huntington's disease




### Journal

Human Molecular Genetics, 22(5)

### ISSN

0964-6906



### Authors

Napoli, Eleonora
Wong, Sarah
Hung, Connie
et al.



### Publication Date

2013-03-01

### DOI

10.1093/hmg/dds503

Peer reviewed

*Human Molecular Genetics, 2013, Vol. 22, No. 5* ***989–1004***
*doi:10.1093/hmg/dds503*
*Advance Access published on November 29, 2012*

# Defective mitochondrial disulfide relay system, altered mitochondrial morphology and function in Huntington's disease

**Eleonora Napoli, Sarah Wong, Connie Hung, Catherine Ross-Inta, Prithvi Bomdica and Cecilia Giulivi***

Department of Molecular Biosciences, University of California Davis, Davis, CA 95616, USA

Received October 5, 2012; Revised November 7, 2012; Accepted November 26, 2012

**A number of studies have been conducted that link mitochondrial dysfunction (MD) to Huntington's disease (HD); however, contradicting results had resulted in a lack of a clear mechanism that links expression of mutant Huntingtin protein and MD. Mouse homozygous (HM) and heterozygous (HT) mutant striatal cells with two or one allele encoding for a mutant huntingtin protein with 111 polyGln repeats showed a significant impairment of the mitochondrial disulfide relay system (MDRS). This system (consisting of two proteins, Gfer and Mia40) is involved in the mitochondrial import of Cys-rich proteins. The Gfer-to-Mia40 ratio was significantly altered in HM cells compared with controls, along with the expression of mitochondrial proteins considered substrates of the MDRS. In progenitors and differentiated neuron-like HM cells, impairment of MDRS were accompanied by deficient oxidative phosphorylation, Complex I, IV and V activities, decreased mtDNA copy number and transcripts, accumulation of mtDNA deletions and changes in mitochondrial morphology, consistent with other MDRS-deficient biological models, thus providing a framework for the energy deficits observed in this HD model. The majority (>90%) of the mitochondrial outcomes exhibited a gene–dose dependency with the expression of mutant Htt. Finally, decreases in the mtDNA copy number, along with the accumulation of mtDNA deletions, provide a mechanism for the progressive neurodegeneration observed in HD patients.**

## INTRODUCTION

Huntington's disease (HD) is a fatal neurodegenerative disorder characterized by psychiatric, cognitive and motor disorders (1). The neuropathology of HD involves the selective dysfunction and death of specific neuronal subpopulations within the central nervous system, in which the most affected cells are the gamma-aminobutyric acid-releasing spiny projecting neurons of the striatum (subcortical brain structure that controls body movement) (2). Disease onset is generally marked by involuntary movements of the face, fingers, feet or thorax (3). Psychiatric symptoms (depression, anxiety, apathy and irritability) are more heterogeneous (4) and can occur up to 20 years before the onset of the choreiform movements. Patients usually die 10–20 years after the first symptoms appear, as currently there is no effective treatment to prevent or delay disease progression.

The human HD gene (also called IT15) contains 67 exons spanning >200 kb. The translated wild-type (WT) huntingtin (Htt) protein is a 350 kDa protein containing a polymorphic stretch of between 6 and 35 Gln residues in its N-terminal domain. When the number of Gln-encoding repeats exceeds 36, the gene encodes a version of huntingtin or mutant huntigtin (mutHtt) that leads to disease (5,6). The mutant protein with the polyGln expansion induces the formation of neuritic, cytoplasmic and nuclear inclusions, leading to dysfunction and finally death of these neurons. Analysis of postmortem brains from patients at the early stages of HD revealed the presence of dystrophic neurites before cell death (7). Early neuropathology has also been detected in mouse models of HD such as electrophysiological and mitochondrial abnormalities and the presence of neuropil aggregates in axons and axon terminals (8).

There is significant evidence that energy production is impaired in HD (9). Impaired glucose metabolism has been

*To whom correspondence should be addressed at: Department of Molecular Biosciences, University of California, One Shields Ave., 1120 Haring Hall, Davis, CA 95616, USA. Email: cgiulivi@ucdavis.edu

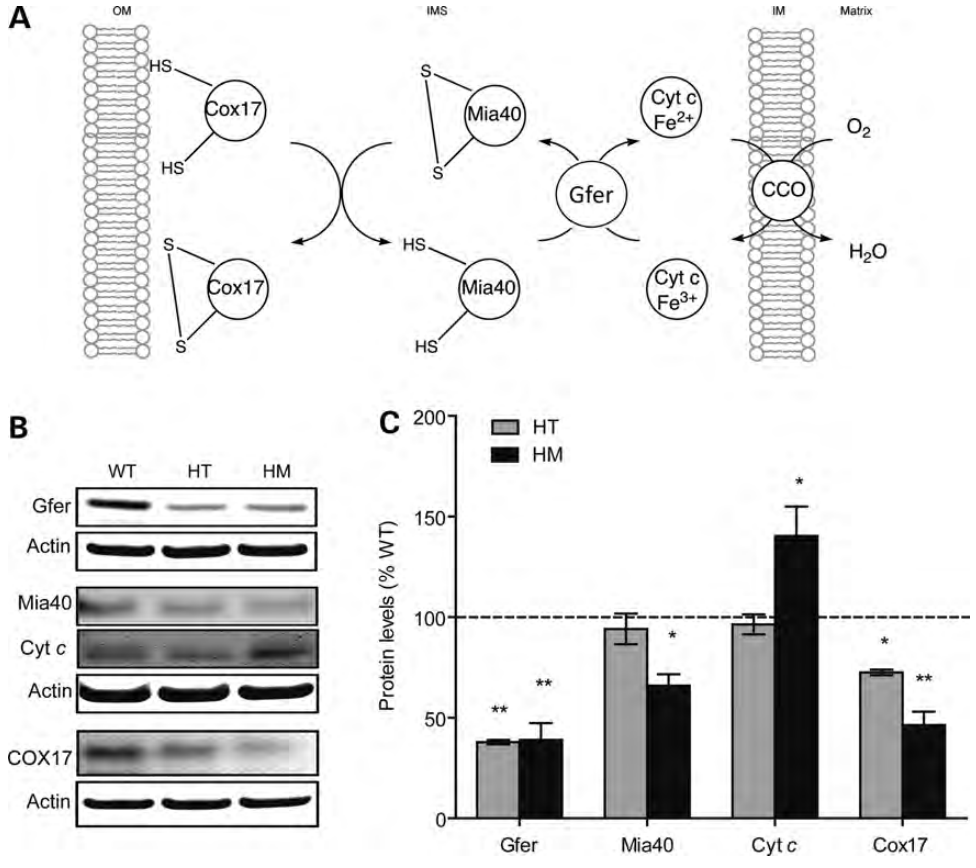


**Figure 1.** Evaluation of the MDRS proteins expression in striatal cells. (**A**). Schematic representation of the MDRS. Mia40 oxidizes the proteins that are imported into the mitochondria trapping them into the intermembrane space, and in turn it gets re-oxidized by Gfer. The transfer of electrons to cytochrome *c* finalizes the restoration of the oxidized form of Gfer. (**B**). Western blots for the indicated proteins were performed on total cell lysates as described under Materials and Methods and Supplementary Material, Table S1. Twenty-five micrograms of proteins were loaded in each lane. Actin was used as a loading control. (**C**). Densitometry of Gfer, Mia40, cytochrome *c* and Cox17, in striatal cells. Data are shown as mean ± SEM. The *P*-values shown are relative to the statistical comparison (ANOVA followed by Bonferroni's post-test) of HT and HM with WT. * $P < 0.05$, ** $P < 0.01$.

observed in striatum of HD patients at early stages of the disease (10–12), striatal hypometabolism has been observed in presymptomatic HD cases (13) and increased lactate levels have been observed in the cortex and basal ganglia from HD patients (5). Others have identified defects in mitochondrial respiratory Complexes II, III and IV in postmortem brain tissues from HD cases with substantial neuronal loss (14–17). However, others indicated that the presence of mutHtt did not impair the activity of respiratory complexes (18–20): Complex activities were not significantly different between mouse striatal neurons with two alleles encoding for a mutHtt with 111 Gln repeats compared with control cells (18), in the striatum of presymptomatic or lower grade HD cases with minimal neuronal loss (19), or in several transgenic HD mouse models (19,20). Other studies reported mitochondrial dysfunction (MD) in brains of transgenic mice (21,22), changes in mitochondrial calcium homeostasis in HD mouse models and in patients' lymphoblasts (23–26), occurrence of a feedback loop between Complex III and the proteasome (27), and deficiency in PGC1-α, possibly leading to an altered mitochondria biogenesis (28).

Mitochondrial and nuclear DNA mutations resulting in mitochondrial diseases have been described in genes encoding for respiratory-chain subunits, oxidative phosphorylation assembly factors, proteins involved in mitochondrial DNA (mtDNA) maintenance, factors related to mitochondrial protein synthesis, biosynthetic enzymes and proteins promoting mitochondrial biogenesis (29). While many of these proteins are synthesized in the cytosol in the form of precursor proteins and post-translationally transported to the mitochondria in an unfolded state, other low molecular weight Cys-containing proteins localized at the IMS require the sequential cooperation of the translocase of the mitochondrial outer membrane (TOM) complex, followed by the mitochondrial disulfide relay system (MDRS) for intramitochondrial import (30) utilizing cytochrome c as the terminal electron acceptor (31).

The MDRS is constituted by two proteins (Fig. 1A), the mitochondrial intermembrane space import and assembly protein 40 (Mia40 also known as coiled-coil-helix-coiled-coil-helix domain-containing protein 4 or CHCHD4) and Gfer (also known as Alr, Erv1, Herv1, HPO). Physiological substrates of the MDRS include many proteins relevant to COX biogenesis (Cox12, Cox17, Cox19, Cox23 (30,32)), several small Tim chaperones (Tim8, Tim9, Tim10 and Tim13 (33,34) and the copper chaperone for superoxide dismutase or Ccs1 (32), in addition to a proposed role in Fe/S traffic in

the cytosolic compartment (35); therefore, a defect in this pathway is likely to result in multiple effects due to a defective import of proteins relevant to Complex IV biogenesis as well as to a number of yet uncharacterized mitochondrial proteins. Defects in the ERV1 gene were initially identified by a temperature-sensitive yeast mutant with a severe defect in oxidative phosphorylation and reduced levels of mitochondrial transcripts (36). In further studies, it was shown that this gene was essential for the maintenance of intact mtDNA (37) as well as mitochondria morphology and distribution (38). Thus, considering that mutHtt is primarily found in the cytoplasm and the initial events leading to the disease may start in this subcellular compartment, we reasoned that an altered MDRS might result in the MD observed in HD.

Despite the wealth of information, to date contradictory results have been obtained in terms of MD, and several issues still remain to be addressed. For instance, what is the role of MDRS in MD? Is the MD based on lower mitochondrial mass and/or dysfunctional MDRS-related substrates? Is there a mutHtt dose dependency? Does a compromised oxidative phosphorylation (OXPHOS) affect the energy status of the HD cell? Does the MD affect differently progenitor and fully differentiated neurons? To address these and other questions, we used mouse striatal neuron progenitors and mature, differentiated neuron-like striatal cells (hereafter called differentiated) in homozygous (HM)-containing two alleles with a 'humanized exon 1' with a 111 polyGln repeat, heterozygous or HT containing one allele with 111 polyGln repeat, and wild-type (WT) cells containing both alleles with a polyGln repeat of 7 (control) neurons.

## RESULTS

### Defective mitochondrial disulfide relay system in HD mitochondria

Defective MDRS reported in yeast expressing a F123S ERV1 mutation (37,38) and in patients with an R194H mutation (39) has been shown to be accompanied by a loss of mtDNA copy number and/or increased deletions, disrupted mitochondrial morphology and MD. Given the similarities between these outcomes and those observed in brain tissues of HD patients (9,14–17), we tested (a) the protein levels of the MDRS components, (b) the mtDNA copy number per cell and mtDNA deletions and (c) mitochondria morphology, (d) mitochondrial activities, coupling between electron transport and ATP production, and mass and (e) the energy status in neuronal HD cells by evaluating ATP levels and by checking ATP-driven cell cycle phases in progenitor and differentiated mouse HM and HT striatal cells with two or one allele encoding for a mutHtt with 111 polyGln repeats.

*Altered ratio of MDRS components in HD*

The protein expression of MDRS components (Gfer, Mia40, cytochrome *c* and the downstream substrate Cox17, Fig. 1A) were evaluated by western blots in neuronal HD cells. While the protein levels of Gfer in both HD cell lines were 38% of control values, those of Mia40 were either not affected (HT) or 67% of control values in HM (Fig. 1B and C). The levels of cytochrome *c* (the terminal electron acceptor of MDRS) in HM were found to be 1.3-fold of controls, maybe as a compensation mechanism to overcome the deficiency in the MDRS. Following the trend of Mia40, the protein level of Cox17 was 72 and 46% of control values in HT and HM, respectively (Fig. 1B and C). Other subunits of Complex IV which do not require the participation of MDRS, such as the mtDNA-encoded subunit III (COXIII), were found not different in HT versus controls but significantly lower in HM (see below), suggesting a disrupted assembly/folding of Complex IV subunits.

Although some substrates for MDRS have been identified, others still remain unknown. To this end, we screened the 40+ subunits of Complex I that fulfilled the requirement for being an MDRS substrate. The sequences were analyzed for the presence of putative IMS-targeting signals (ITSs) characteristic of MDRS substrates, *i.e.*, by defining an ITS as a stretch of at least nine amino acids upstream or downstream of any Cys of the $CX_9CX_nCX_9C$ motif, and having one aromatic and one hydrophobic amino acid (or two aromatic amino acids) four and seven residues distant from the Cys (40). *In silico* searching resulted in three candidates, NDUFB7, NDUFA8 and NDUFS5, consistent with those predicted for Complex I across several species (41,42). Western blot analysis indicated that levels of NDUFB7 and NDUFS5 in HD cells were 54% and 140% of controls, with no difference between HT and HM (Fig. 2). (Note: the commercially available anti-NDUFA8 antibody was tested at multiple dilutions (from 1:1000 to up to 1:300) but no band was visualized with any of the cell lines).

To test whether the altered expression of NDUFB7 and NDUFS5 could affect that of other Complex I subunits, given that the assembly of this complex is performed through multiple stages involving the formation of subcomplexes (43,44), western bots were run for Complex I subunits representing all three sub-complexes of Complex I (I-alpha, I-beta and I-lambda). No significant changes in Complex I subunits were detected in HT, besides NDUFB7 and NDUFS5 (Fig. 2). In HM cells, the protein expression of NDUFA9, GRIM19 (or NDUFA13) and NDUFS3 was decreased by 47, 47 and 69% in HM, whereas that of NDUFS4 was increased by 217% (Fig. 2). These results clearly suggested a disrupted protein assembly/folding consistent with a disrupted MDRS with altered expression of Complex I subunits, more exacerbated in HM than HT. It is interesting to note that NDUFS4 protein expression is higher in HM than in WT, since this subunit is a target for phosphorylation/dephosphorylation (45,46), process which may regulate the reversible switch of Complex I between active and de-active conformations dependent on the cell respiratory status (45,46).

*Decreases in the mtDNA copy number and mitochondrial transcripts accompanied by increases in mtDNA deletions in a mutHtt-dose and passage number dependence*

The mtDNA copy number in controls was 305 $\pm$ 13 from passages 6 to 11, showing a statistically significant decrease by 31% ($P < 0.05$) only at passage 13 (Fig. 3A). In HT cells, the mtDNA copy number was lower than controls at all passage numbers (by 18 $\pm$ 3%, combined $P < 0.0001$) and a statistically significant decrease was observed at passages 10

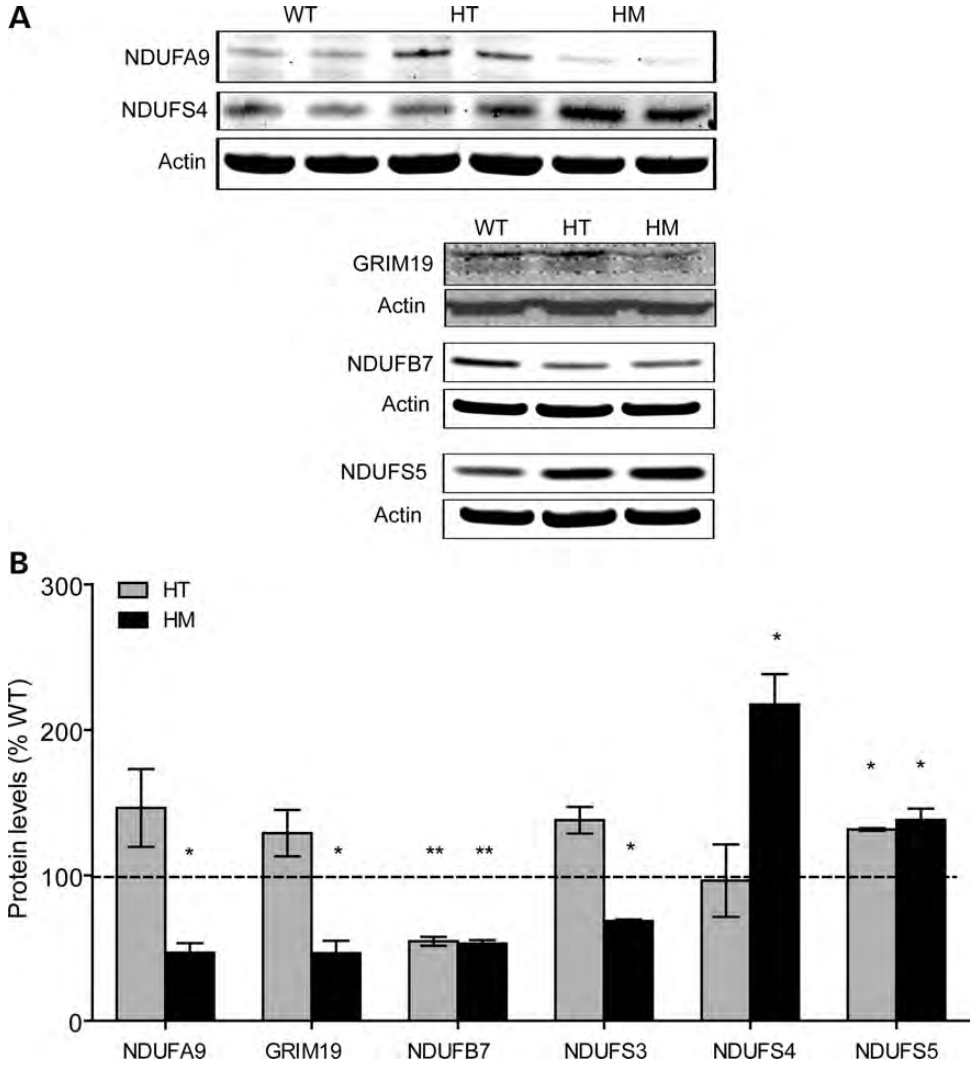


**Figure 2.** Expression of mitochondrial complex I subunits in striatal cells. (**A**). Western blots for the indicated subunits were performed on total cell lysates as described under Materials and Methods section and Supplementary Methods. Actin was used as a loading control. Details and dilutions of the antibodies used are reported in Supplementary Material, Table S1. (**B**). Densitometry of NDUFA9, GRIM19, NDUFB7, NDUFS3, NDUFS4, NDUFS5 was performed with the Image Studio 2.0 software. Data are shown as mean ± SEM. The *P*-values shown are relative to the statistical comparison (ANOVA followed by Bonferroni's post-test) of HT and HM with WT. * $P < 0.05$, ** $P < 0.01$.

and 13 relative to that at passage 6 (by 19 and 27%, respectively, $P < 0.05$ and $P < 0.01$). In HM, mtDNA copy number was significantly lower than WT at all passage numbers (by an average $34 \pm 4\%$, combined $P < 0.0001$, Fig. 3A). At early passages (6–7), the mtDNA copy number in HM was similar to that of HT, with the difference that the copy number started declining as early as passage 9 (by 20% relative to HM passage 6, $P < 0.05$), reaching a plateau at passages 10 and higher ($49 \pm 1\%$ decrease at passages 11–13 compared with passage 6, $P < 0.0005$). Although this mtDNA copy number was only 50% of control values at passage 13, these levels were above the threshold for considering a mtDNA depletion syndrome (30% or lower (47,48)).

None of the proteins so far identified as substrates for MDRS belong directly to mtDNA replication/maintenance; however, it is important to note that the mtDNA replication starts near or at the inner membrane (49), thus disruption or changes in the IM architecture may also affect mtDNA replication (37). In this regard, the transcript level of Chchd10, a protein containing the $CX_9CX_9C_9X_9C$ motif which was found to be a potential MDRS substrate (42), was significantly downregulated in HM (−3.93 and −6.02 compared with WT and HT, respectively; $P < 0.05$), and although a definite role for this protein has not yet been reported (50), another mitochondrial coiled-helix-coiled-helix protein Chchd3, with the motif $CX_9CX_{10}CX_9C$ and also a potential substrate for MDRS (42), has been found to have a critical role in cristae maintenance and mitochondrial function (51).

No significant accumulated deletions—as judged by the CYTB/ND1 ratios—were observed in control cells between passages 9 and 13 (from 0% to 2.6%; Fig. 3B). However, mtDNA deletions were evident at passage 9 only in HM (3.5%, Fig. 3B), and more drastically at passage 13 for both HM and HT (11.4 and 27.4% for HT and HM, respectively;

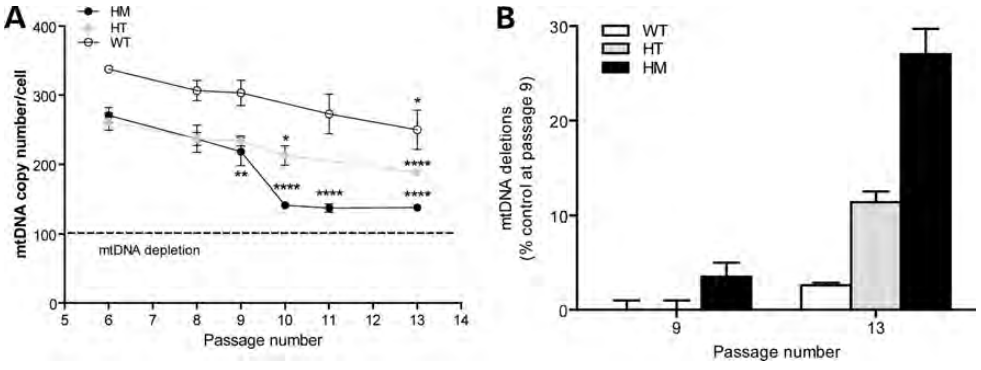


**Figure 3.** Effect of passage number on the mtDNA copy number and deletions. (**A**). MtDNA copy number was evaluated in WT, HT and HM cells at passages 6–13. Asterisks represent statistically significant differences relative to passage 6 for each individual cell line. $^{*}P < 0.05$, $^{**}P < 0.01$, $^{****}P < 0.0005$ evaluated with ANOVA followed by Bonferroni's post-test. (**B**). MtDNA microdeletions at passage 9 and 13 in striatal cells. Values are shown as percentage of control values at passage 9.

Fig. 3B) relative to controls. Thus, these results indicated that mtDNA deletions accumulated with passage number and in a mutHtt-dose dependency.

To evaluate the effect of the quality of the template and the number of copies on transcription, mtDNA transcripts (10 out of 13 protein-encoding genes) were evaluated by qPCR. The level of transcripts was significantly lower in HM ($69 \pm 4\%$ of WT, $P < 0.0001$) and HT ($67 \pm 4\%$ of WT, $P < 0.0001$) at passages 9–11 than controls (Supplementary Material, Fig. S3). At passage 14, mitochondrial transcripts in HM and HT cells were, respectively, $22 \pm 4\%$ ($P < 0.0001$) and $11 \pm 2\%$ ($P < 0.0001$) of the ones measured in the same cell line at passages 9–11 (Supplementary Material, Fig. S3). These results indicated that the average of the levels of the mtDNA-encoded transcripts decreased with passage number, following the trend observed for microdeletions of mtDNA.

The accumulation of mtDNA deletions might be a reflection of a defective clearance of damaged mitochondria, process accomplished via the selective autophagy named mitophagy (52). This process requires PARK2 recruitment to dysfunctional mitochondria with a stabilized PINK1 at the outer membrane (OM) to initiate their degradation (53). While no changes in gene expression for PARK2 or PINK1 were obtained by qPCR, significant decreases in gene expression were obtained for UCHL1 or PARK5 and LRRK2 or PARK8. The UCHL1 transcript levels were 5- to 6-fold lower in HM compared with controls, and the levels were ~10-fold lower in HM compared with HT ($P < 0.001$). The LRRK2 transcript levels were $-6.54$ in HM and $-2.98$ in HT of controls ($P < 0.001$). As defects in PARK2 and PINK1 are the cause of Parkinson disease types 2 and 6, respectively, Parkinson type 8 is associated with defects in LRRK2, a protein involved in autophagy localized at mitochondrial outer membrane, (54), and Parkinson disease type 5 is associated with defects in UCHL1, an ubiquitin carboxyl-terminal hydrolase. Given that polymorphisms in UCHL1 have been described as risk factors for the age of HD onset (55), decreases in UCHL1 and/or LRRK2 might trigger a decreased clearance of defective mitochondria and accumulation of damaged organelles.

*Altered mitochondrial morphology in HD cells*

The critical differences in the morphology of mitochondria from HD cells, evaluated by using MitoTracker Deep Red (56), were observed compared with control cells (Fig. 4A and B). In control cells, the majority of mitochondria were organized as an extended network of tubular structures (57) (Fig. 4A and B). However, the mitochondrial network of HD cells appeared disrupted and the mitochondrial morphology appeared either fragmented or circular (or 'doughnut-like'; Fig. 4A and B), in agreement with other reports on HD-affected rat cortical neurons and fibroblasts (58) and with the mitochondrial morphology observed in yeast ERV1 mutants (38).

The increase in circular mitochondria was 4.5-fold and 5.5-fold for HT and HM cells (Table 1). Although the increase in circular mitochondria could be mainly accounted for the decrease in tubular mitochondria, more fragmented mitochondria were also observed in HD cells (2.5-fold of controls; Table 1). Upon differentiation, HD cells showed the same mitochondrial pattern as progenitor cells, with fragmented and circular mitochondria still evident in HT and HM cells (Fig. 4).

*Complex I, Complex IV and Complex V affected in HD with a mutHtt-dose dependency*

Given the MDRS deficits observed above, individual complex activities were evaluated to identify generalized versus specific defects at the electron transport chain (ETC) in both progenitor and fully differentiated neurons. Regardless of the differentiation process, HT cells had lower Complex I activity, as judged by NADH-quinone oxidoreductase activity (NQR) ($58 \pm 8\%$ in average) and NADH-ferricyanide oxidoreductase activity (NFR) ($46 \pm 10\%$ in average, not shown), relative to controls (Table 2). No differences in succinate-cytochrome *c* reductase activity (SCCR) (Complexes II and III) or ATPase mitochondrial ATP hydrolyzing activity activities were recorded in HT, progenitor or differentiated cells (Table 2). Despite having lower expression of Gfer and Cox17, the cytochrome c oxidase (CCO) activity in HT was 2.2-fold of control values, suggesting that (i) these lower protein expressions were not enough to trigger a lower CCO activity and (ii) the increase in CCO activity was probably triggered in an attempt to overcome the deficiency at the level of Complex I. In agreement with these observations, myoblasts from patients harboring the R194H Gfer point mutation resulted in a significant lower colocalization of Gfer with mitochondria accompanied by decreases in muscle Complexes I (46.5%), II

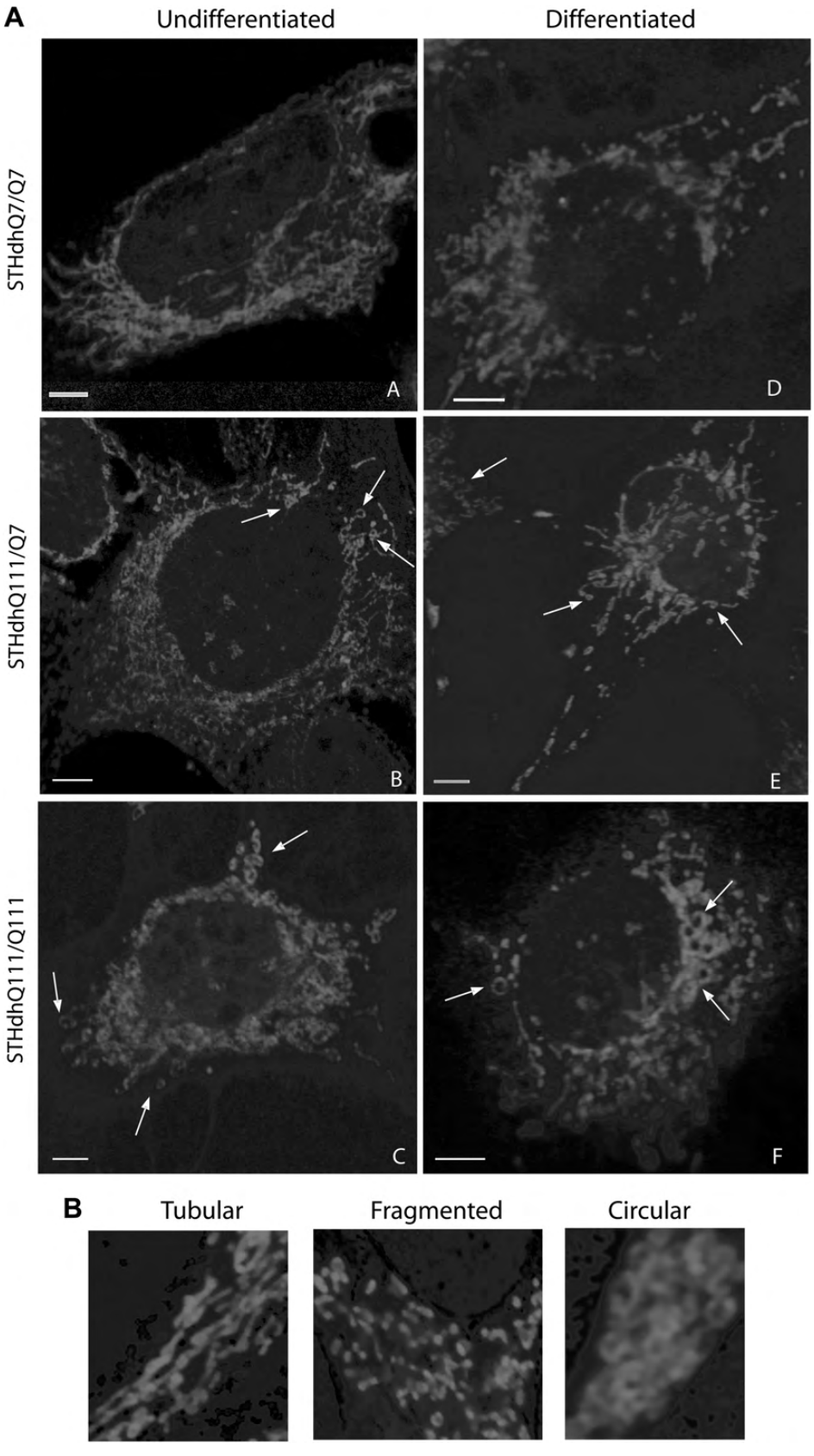


**Figure 4.** Mitochondrial morphology in progenitor and differentiated striatal cells. (**A**). Confocal images of progenitors and differentiated striatal cells probed with MitoTracker Deep Red FM. Cells were plated onto polylisine-coated coverslips and then stained as described in the Materials and Methods section. Images were taken using an Olympus FV1000 laser scanning confocal microscope at 60× magnification and zooms variable between 2.0 and 3.0. Scale bar = 10 nm. White arrows identify some of the circular mitochondria. (**B**). Details (60×, zoom 4.0) of tubular, fragmented and circular mitochondria in progenitor striatal cells.

**Table 1.** Mitochondria morphology in striatal cells

| Cell line | Mitochondria morphology (%) Tubular | Circular | Fragmented | Other |
|---|---|---|---|---|
| WT | $74 \pm 1^{a,b}$ | $11.3 \pm 0.7^{c,d}$ | $7.9 \pm 0.6^{e,f}$ | $6.7 \pm 0.4^{g,h}$ |
| HT | $19.7 \pm 0.8^{a}$ | $49.7 \pm 0.5^{c}$ | $16.8 \pm 0.7^{e}$ | $13.7 \pm 0.8^{g}$ |
| HM | $8.9 \pm 0.7^{b}$ | $61.2 \pm 0.7^{d}$ | $20.5 \pm 0.8^{f}$ | $9.4 \pm 0.5^{h}$ |

Numbers with the same superscripts were significantly different from each other with $P = 4 \times 10^{-28}$ (a), $4 \times 10^{-31}$ (b), $2 \times 10^{-28}$ (c), $6 \times 10^{-34}$ (d), $2 \times 10^{-10}$ (e), $4 \times 10^{-14}$ (f), $5 \times 10^{-8}$ (g)and $3 \times 10^{-5}$ (h).

(62.1%) and IV (44.8%), indicating that a significant decrease in MDRS activity might be required to observe a decline in Complexes II and IV. However, we cannot exclude tissue-specific differences of the MDRS pathway in myoblasts versus neurons. In this regard, OXPHOS in brain, liver and kidney is mainly controlled at the phosphorylation level by ATP synthase and a phosphate carrier, whereas in muscle and heart, the control is exerted at the level of the respiratory chain (59); thus, deficits in MDRS in neurons may trigger additional defects such as a lower ATPase activity. This prediction was confirmed experimentally in HM cells (see below).

Consistent with the prediction of a more affected MDRS in HM, Complex I and IV activities were significantly lower than controls, regardless of the differentiation stage (NQR = 64%, Table 2; NFR = 64%, not shown; CCO = 46%, Table 2). A lack of support for post-translational modifications of Complex I resulting in activity loss was attributed to the lack of Complex I activity recovery by preincubation with 1 mM dithiothreitol (DTT) (as judged by NQR and NFR activities), indicating that the impaired activity was not due to the oxidation of thiols and/or formation of *S*-nitrosothiols (60) from increased oxidative stress (see below). CCO activity showed a significant decrease in progenitor and differentiated HM ($46 \pm 7\%$ in average; Table 2), accompanied by a 36% decrease in the protein expression of COXIII (Fig. 5A). No changes in SCCR were observed in HM cells in contrast with a mouse model of HD, in which administration of 3-nitroproprionic acid, a mitochondrial Complex II inhibitor, was found to replicate many of the pathological and clinical features of HD (61). On the other hand, this model may very likely reproduce the deficit in Complex II-III (along with Complex IV) characterizing advanced stages of the disease, as observed on caudate and putamen of HD patients at stages 3 and 4 (15,16).

Thus, an altered pattern of Complex I subunits seems to account for its decreased activity in HD cells, originated from a defective MDRS. Although both HD cells presented lower Cox17 expression (Fig. 1), the further reduction of Cox17 levels observed in HM versus HT (by 40%; Fig. 1) seems to point to a limiting step in the assembly of a functional CCO Complex that impacts HM but not HT.

*MDRS deficits and other mechanisms contribute to ATPase activity decline in HD*. The Complex V activity in HM was lower than controls and HT (ATPase = 63%), although no proteins directly related to ATPase have been found to be potential MDRS' substrates, nDNA-encoded subunits with (e.g. alpha and beta subunits) or without (e.g. subunit d) N-terminal pre-sequences may be impacted by a defective MDRS resulting in an altered downstream import pathway via the disruption of small Tim chaperones, known MDRS substrates (see Discussion). In addition, other mechanisms that may have contributed to the decline in ATPase activity were explored. Among them, the role of OM-bound mutHtt which may impact the assembly/import of ATPase subunits, the occurrence of $F_1F_o$-ATPase inhibitor ($IF_1$) to limit ATP loss and Tyr nitration as a marker for oxidative stress.

First, the protein level of Complex V subunit alpha (but not that of beta) was found different in HM from both HT and WT (Fig. 5B) resulting in an alpha-to-beta ratio different from that of WT, suggesting that there is an accumulation of beta subunits not incorporated into an 'active' $F_1$ with the correct stoichiometry (1:1). We hypothesize that attachment of mutHtt to OM, in a gene–dose manner, may result in lower import/folding of nDNA-encoded subunits for Complex V, and as such, result in lower ATPase activity. Indeed, it has been reported that (i) binding of mutHtt to OM increases mitochondria susceptibility to calcium-induced permeability transition pore opening and cytochrome *c* release (25) and (ii) the interaction of mutHtt with the OM protein Drp1 increases mitochondrial fragmentation and impairs mitochondrial biogenesis (62). In other reports, it has been shown that blocking mitochondrial contact sites by, for example, overexpressed precursor mitochondrial proteins, leads to defective transport, (63) whereas increases in cyclin D1, such as those observed in leukemia, seem to outcompete endogenous HK2 for VDAC binding at the OM (64). To this end, the total and mitochondria-bound WT and mutHtt were evaluated by immunofluorescence in controls, HT and HM cells (Supplementary Material, Fig. S4A, B). In a gene–dose dependency, a lower co-localization of WT Htt with mitochondria (HT = 79% of controls; $P < 0.001$) was accompanied by an increase in the co-localization of mutHtt with mitochondria (HT = 45% of HM; $P < 0.0001$). In agreement with these findings, the levels of the voltage-dependent anion channel (VDAC) OM protein were 80 and 50% of controls, respectively, in HT and HM (Supplementary Material, Fig. S4C), a further confirmation of the mutHtt-dependent altered import/assembly of mitochondrial proteins (of note, the decrease of VDAC levels in HM cells were 1.5-fold lower than the observed decrease in mitochondrial mass, see below).

Second, the expression of the $IF_1$ was significantly higher in HT (15-fold) and HM (10-fold) HD than WT (Fig. 5C). This increase may reflect an attempt to limit ATP depletion when the mitochondrial membrane potential falls below a threshold and the $F_1F_o$-ATP synthase starts hydrolyzing ATP to pump protons out of the mitochondrial matrix (65,66). Increases in $IF_1$ halt or decrease the ATP hydrolysis (or ATPase activity) without affecting the ATP synthesis activity of Complex V (66). Although $IF_1$ protein expression was higher in both HT and HM, whereas the activity was affected only in HM, it is worth noting that the $IF_1$ protein only binds to the ATP synthase under specific conditions of acidic pH (67), conditions not always present in mitochondria (67), as it could be in the case of HT in which the MD is less evident than in HM.

Finally, Tyr nitration, as a post-translational modification of Complex V subunits, did not seem to have a role in the decline of ATPase activity (68). Although (i) other post-translational

**Table 2.** Mitochondrial mass and OXPHOS function in progenitor and differentiated HD cells

| Outcome | Progenitor Control | HT | HM | Differentiated Control | HT | HM |
|---|---|---|---|---|---|---|
| Mitotracker staining (FU) | 45 ± 2 | 34 ± 1*** | 30 ± 1*** | 41 ± 2 | 31 ± 1*** | 28 ± 1*** |
| CS[a] | 73 ± 1 | 56 ± 4** | 50 ± 3**** | 73 ± 4 | 50 ± 5*** | 46 ± 4**** |
| NADH Oxidase[b,c] | 0.084 ± 0.004 | 0.033 ± 0.004**** | 0.019 ± 0.001**** | 0.067 ± 0.001 | 0.037 ± 0.003** | 0.023 ± 0.005* |
| Succinate Oxidase[b,c] | 0.070 ± 0.003 | 0.087 ± 0.006 | 0.023 ± 0.004*** | 0.048 ± 0.001 | 0.063 ± 0.005 | 0.025 ± 0.008* |
| CCO[b,c] | 0.069 ± 0.001 | 0.173 ± 0.012**** | 0.035 ± 0.003* | 0.082 ± 0.001 | 0.154 ± 0.020*** | 0.034 ± 0.001* |
| NQR[a,c] | 1.35 ± 0.07 | 0.70 ± 0.05*** | 0.92 ± 0.06** | 0.79 ± 0.08 | 0.50 ± 0.04* | 0.47 ± 0.06* |
| SCCR[a,c] | 0.030 ± 0.003 | 0.033 ± 0.003 | 0.023 ± 0.002 | 0.022 ± 0.001 | 0.029 ± 0.004 | 0.03 ± 0.001 |
| ATPase[a,c] | 0.31 ± 0.04 | 0.31 ± 0.05 | 0.17 ± 0.02* | 0.32 ± 0.04 | 0.37 ± 0.07 | 0.22 ± 0.02* |
| RCRu | 13.0 ± 1.0 | 7.5 ± 0.2** | 5.3 ± 0.6*** | 4.7 ± 0.4 | 2.5 ± 0.2* | 1.8 ± 0.5** |

[a]Measured spectrophotometrically. All rates were expressed as nmol × (min × $10^6$ cells)$^{-1}$ and reported as mean ± SEM.
[b]Measured polarographically and reported as mean ± SEM.
[c]normalized by CS.
Significant with *$P < 0.05$; **$P < 0.01$; ***$P < 0.005$; ****$P < 0.001$ relative to control.

modifications cannot be excluded, (ii) increased oxidative stress was observed in HD cells (steady-state concentrations of hydrogen peroxide in progenitor control, HT and HM were 44 ± 6, 69 ± 10 and 285 ± 18 nM, respectively; $P < 0.01$), and (iii) the levels of nitrated beta-ATPase in HD cells were significantly higher than WT (7.5- and 9-fold higher in HM and HT, respectively, of WT, Supplementary Material, Fig. S5), a similar level of nitration did not seem to account for the decreased Complex V activity observed in HM only.

## Decreased oxygen consumption and coupled respiration in HD mitochondria

To assess the effect of the deficits on complex activities, the oxygen consumption rates were followed in permeabilized HD cells. The use of permeabilized cells overcomes potential issues with substrate permeability at the plasma membrane and/or access to mitochondria. NADH-oxidase activity (Complex I → III → IV → V) in the presence of ADP (phosphorylating conditions) was significantly decreased in HD cells (39 and 23% of control values for HT and HM, respectively; Table 1). Succinate oxidase (Complex II → III → IV → V) supplemented with ADP showed significant deficits only in HM cells (33% of WT; Table 1). Deficits in NADH- and succinate-oxidase activities were also observed in differentiated HD cells, at comparable levels with those observed previously with progenitors (NADH oxidase: 55 and 34% of control values for HT and HM, respectively; succinate oxidase: 52% of control values for HM, Table 2). These results indicated in HM a defect at the level of Complex I and in the segment of Complexes III–V, whereas in HT, the defects were only observed in Complex I, in agreement with the results obtained with the individual evaluation of complex actvities.

The coupling of electron transport to ATP synthesis (evaluated by the respiratory control ratio or RCR) was evaluated in HD cells. Control cells exhibited a high RCRu (Table 2); conversely, a significant percentage of mitochondria were uncoupled in both HD cells (46 and 64%, respectively, in HT and HM). Consistent with the results obtained with progenitor cells, the RCRu of differentiated control and HD neurons was not affected by the differentiation process, remaining at values similar to those of the progenitor cells (53 and 38% of WT for HT and HM, respectively; Table 2).

## Mitochondrial OXPHOS is more affected in HD than mitochondrial mass

To ascertain the putative effect of lower mitochondrial mass in HD on OXPHOS, three markers of mitochondrial mass were assessed: citrate synthase (CS) activity, mitochondria density per cell area and mtDNA copy number per cell. The CS activity was found to be significantly lower in progenitor HD cells (72 and 65% of WT for HT and HM, respectively; Table 2). In parallel experiments, confocal microscopy was performed to evaluate mitochondrial mass and function in living cells by staining with Mitotracker Deep Red. The fluorescence of the dye normalized to the total cell area indicated a 25 and 33% decrease in functional mitochondria for progenitor HT and HM, respectively, compared with WT (Table 2 and Supplementary Material, Fig. S6). Similar results were obtained for differentiated HD cells for both citrate synthase and confocal microscopy (74 ± 1% and 60 ± 1% of WT for HT and HM, respectively, for both outcomes; Table 2 and Supplementary Material, Fig. S6).

The mtDNA copy number—as observed before—decreased in HD cells (by 20 and 34% in HT and HM; Fig. 3). These decreases were comparable with those observed with CS activity and by confocal microscopy (by 25–28% in HT and by 33–40% in HM). The decrease in mtDNA copy numbers associated with increased mtDNA deletions observed in HD was consistent with that observed in patients carrying an R194H mutation in Gfer (39).

Although the mitochondrial mass decreased in HD cells (by 25 and 39% on average in HT and HM, respectively), this decrease was significantly less than that of some of the mitochondrial outcomes tested above. In HD cells, the expression of Gfer decreased by 62% and the expression of NDUFB7 by 50%. Complex activities, NADH- and succinate oxidase were 50–80% of WT on average after normalization by citrate synthase (Table 2). Furthermore, in HM cells, the average expression of Cox17, NDUFA9, GRIM19 and alpha-ATPase was decreased by 56 ± 4% to WT, suggesting

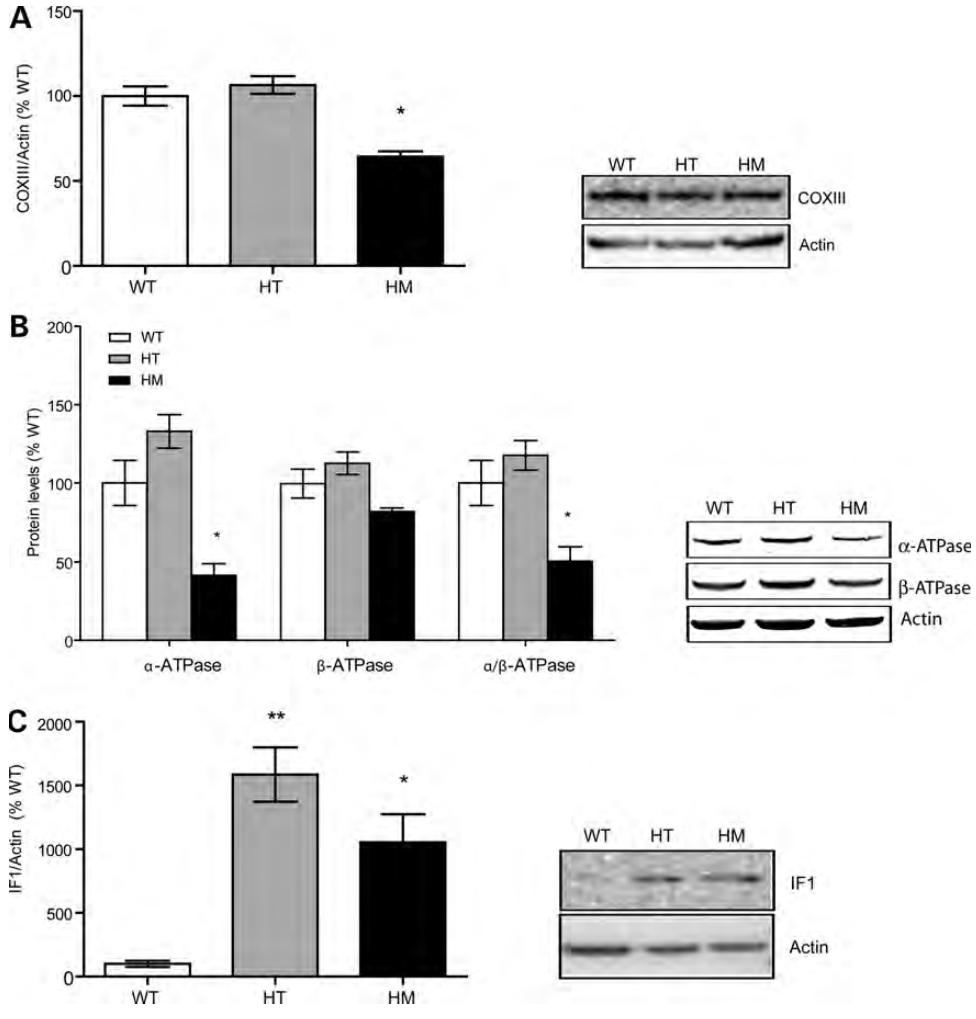


**Figure 5.** Expression of mitochondrial complex IV and V subunits in striatal cells. Densitometry and representative western blot for (**A**) Complex IV subunit III, (**B**) Complex V subunit alpha and beta and (**C**) Complex V subunit IF1 were performed on total cell lysates as described under Materials and Methods section and Supplementary Material, Table S1. Thirty micrograms of total proteins were loaded per lane and actin was used as a loading control. Densitometry was evaluated with the use of the Image Studio 2.0 software. Data are shown as mean ± SEM. The *P*-values are relative to the statistical comparison (ANOVA followed by Bonferroni's post-test) of HT and HM with WT. $^{*}P < 0.05$, $^{**}P < 0.01$.

that the implication of a defective MDRS leads to MD more than a decreased mitochondrial biogenesis and/or mass in contrast with other reports in which decreases in mass seem to be as relevant as deficits in function (9,18).

### HD striatal cells exhibit energy deficits detectable by longer doubling time and $G_1$-S cell cycle arrest

A unifying hypothesis linking chronic ATP depletion and oxidative stress in HD had emerged in recent years (9). To test whether the observed disrupted OXPHOS, mitochondrial morphology and mtDNA maintenance observed in HD cells could result in energy deficits, total and mitochondrial ATP levels were recorded in progenitors and differentiated striatal cells. Total ATP production in HT and HM was 53% and 38%, respectively, of WT (average of progenitors and differentiated cells, Table 3). Mitochondrial ATP levels (evaluated as the difference between total ATP production and the oligomycin-resistant one) were, respectively, 73 and 41% of WT (average of progenitors and differentiated, Table 3).

To evaluate whether these lower levels of ATP could be considered as energy deficits in HD, and given that decreases in mitochondrial ATP production blocks $G_1$-to-S phase progression in flies (4), without necessarily affecting viability, we evaluated the doubling time (DT) and the cell cycle progression in HD cells. In growth media, only HM showed a longer DT than controls (1.4-fold; 33 ± 1 h; $P < 0.05$). Analysis of the cell cycle phases carried out with the fluorescence ubiquitination cell cycle indicator (FUCCI) cell cycle sensor after the first round of division showed a significant increase of the number of cells in $G_1$-S for HM only (7.3-fold and 4.3-fold higher than WT and HT, with $P < 0.01$ and $P < 0.5$, respectively; Supplementary Material, Fig. S7). Thus, these results indicated that the longer DT observed in HM cells could be attributed to an increased block in the $G_1$-S phase. While we cannot exclude other contributing factors or mechanisms (58,62,69), $G_1$-S arrest is triggered by metabolic stress

**Table 3.** Total and mitochondrial ATP levels in progenitors and differentiated striatal cells

| | Progenitors | | Differentiated | |
|---|---|---|---|---|
| | Total ATP | Mitochondrial ATP | Total ATP | Mitochondrial ATP |
| WT | 2.35 ± 0.34 | 1.01 ± 0.19*** | 2.32 ± 0.32 | 1.02 ± 0.21*** |
| HT | 1.35 ± 0.31 | 0.77 ± 0.11*** | 1.17 ± 0.01 | 0.72 ± 0.01*** |
| *P*-value versus WT | $P < 0.05$ | $P < 0.01$ | $P < 0.01$ | – |
| HM | 0.89 ± 0.02 | 0.42 ± 0.02*** | 0.89 ± 0.01 | 0.42 ± 0.01*** |
| *P*-value versus WT | $P < 0.01$ | $P < 0.01$ | $P < 0.01$ | $P < 0.05$ |
| *P*-value versus HT | – | $P < 0.01$ | – | – |

ATP concentrations were expressed as nmol/million cells. Data are mean ± SEM of at least two measurements in duplicate. ***$P < 0.001$ versus correspondent total ATP levels evaluated by Student's *t*-test.
Statistical analysis of the comparison among HT, HM and WT was performed with ANOVA followed by Bonferroni's post-test. Mitochondrial ATP levels were evaluated as described in the Materials and Methods section.

checkpoint of the cycle that is controlled by the activation of LKB1/NUAK1 (70) promoting the phosphorylation of p53 at S15 and S392 (71), modifications that prevent its degradation, resulting in the cellular accumulation of p53 and a longer cell cycle.

Energy deficits seem to be contributing to the phenotype in HM but not in HT at passages 9–11; however, at higher passages, this deficit may extend to HT as well. In addition, although mitochondria are fundamental at providing ATP via OXPHOS, we cannot exclude other critical processes such as heme biosynthesis, one-carbon metabolism, some steps of amino acid synthesis and degradation, which may result affected in both HT and HM.

## DISCUSSION

The results presented in this study indicate that there is a deficit in the MDRS which includes lower protein expression of Gfer (HM = HT) and Mia40 (HM), and the downstream target Cox17 (HM > HT), altered expression of Complex I subunits (HM > HT), disrupted mitochondrial morphology (HM > HT), lower mtDNA copy number and increased deletions (HM > HT), lower OXPHOS, Complex I, IV and V activities and ATP levels (HM > HT), and increased oxidative stress (HM = HT). These outcomes seemed to follow a gene–dose and passage number dependency, i.e. more pronounced in HM than HT and with increasing passage number. It is worth noting that the altered protein expression of the MDRS components, as observed in HD, might underestimate the magnitude of the defect, for oxidation of critical Cys at Mia40 via increased oxidative stress, as it is observed in these cells expressing mutHtt, might result in even lower MDRS activities than those expected solely on protein expression.

Several studies have shown evidence that energy production is impaired in HD. Impaired glucose metabolism has been observed in striatum of HD patients at early stages of the disease (10–12) and, some groups have also reported deficits in mitochondrial Complex I in platelets and muscle of HD patients (72,73), and Complexes II, III and IV in postmortem brain tissue from HD cases with substantial neuronal loss (14–17). However, other reports indicated that the presence of mutHtt does not seem to impair the activity of the respiratory Complexes in striatum and cerebral cortex of transgenic mice (19,20). Previous studies on HM mouse striatal cells showed decreased oxygen consumption and decreased ATP levels not accompanied by impaired ETC activities (18); others using the same mouse HM and control cells and, in one human fibroblast cell line, suggested a role for mutHtt-mediated oxidative damage leading to mtDNA damage and decrease in the general spare respiratory capacity in HD cells (74). Our study conducted using the same mouse model, but including the HT and differentiated cells for the first time, confirmed some of the outcomes (lower ATP production), in addition to providing evidence for a significant impairment of MDRS, OXPHOS, Complex I, IV and V activities, decreased mtDNA copy number and transcripts, and increased deletions in progenitors and differentiated HM cells, thus providing a framework for the observed ATP production impairment. The discrepancies between our results and the ones previously obtained using the same cellular model (18) may lie on the different methodologies used for the preparation of the homogenates for enzymatic assays (i.e., use of protease and phosphatase inhibitors, this study). In addition, we demonstrated the importance of testing STHdh striatal cells at different passage numbers to unveil accumulated damage, which may have been overlooked at early passages. In this regard, a dysfunctional mechanism involving UCHL1 and LRRK2 could explain the accumulation of damaged mitochondria that originates in either the decreased transcript levels and/or defective insertion at the outer membrane caused by the mutHtt attached to mitochondria. This 'resistance' to degradation could be interpreted as an attempt to sustain ATP levels when glycolysis has been significantly affected (decreases in ATP by glycolysis were by 60% whereas those from mitochondria were by 20% in HT and by 60% in HM). Indeed, during starvation, the levels increase and activate protein kinase A (PKA, which in turn, may phosphorylate the pro-fission dynamin-related protein 1 (DRP1), which is therefore retained in the cytoplasm, leading to unopposed mitochondrial fusion. Elongated mitochondria are spared from autophagic degradation, possess more cristae, increased levels of dimerization and activity of ATP synthase, and maintain ATP production (75). Similar to those observations, mitochondria showed a typical doughnut-like shape, which seem to result from a head–tail collapse of elongated mitochondria and halted autophagic response, contrary to that study, with no changes (HT) or lower (HM) ATPase activity.

Three main conclusions can be drawn from this study: (i) disrupted MDRS seems to underlie most of the observed mitochondrial changes, both directly (as noted at the levels of Complexes I and IV for subunits that are MDRS substrates) and indirectly (ATPase). In this last instance, defects in MDRS may lead to deficits in MDRS substrate proteins Tim8, 9, 10 and 13 (76,77). Some of these chaperones are part of the TIM22 complex (Tim9, Tim10, Tim12), which is responsible for translocation/insertion of carriers as well as for Tim23 and Tim17 (78). Tim23 is an essential component of TIM23 complex whose function is to import precursors with an N-terminal pre-sequence (77), such as the ATPase

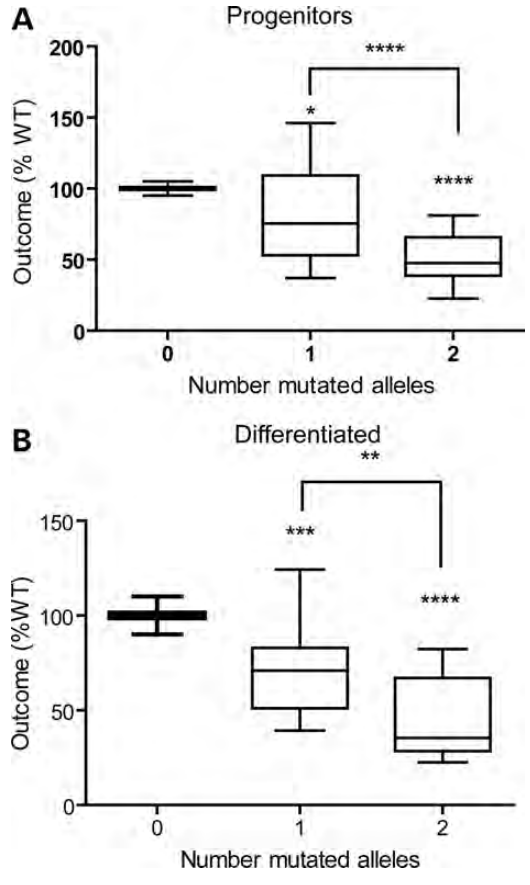


**Figure 6.** Mutant Htt gene dosage effect on mitochondrial outcomes. Box and whiskers representation of the gene–dose dependency observed for 20 of the 27 and 13 of the 15 outcomes tested in progenitors and differentiated striatal cells, respectively. Whiskers represent minimum and maximum values. Outcomes were expressed as percentages of control values and plotted versus the number of mutants Htt alleles. $R^2 = 0.987$ and 0.998 for progenitors and differentiated cells, respectively. Outcomes that showed a statistically significant increase in HD cells compared with WT (CCO, ROS (reactive oxygen species production), IF1, nitrated beta-ATPase, NDUFS4, NDUFS5 and cytochrome *c*) were not included in this analysis. *P*-values are relative to the statistical comparison (ANOVA followed by Bonferroni's post test for multiple comparisons) between HT or HM and WT (asterisks), and between HT and HM (brackets). $^{*}P < 0.05$, $^{**}P < 0.01$, $^{***}P < 0.005$, $^{****}P < 0.0001$.

beta subunit (79). Thus, it is possible that an initial disruption of MDRS leads to an altered downstream import pathway. In support of this notion, the severity of the Mohr–Tranebjaerg syndrome seems to be underlined by impaired biogenesis of the TIM23 complex as a result of dysfunctional Tim8 (deafness dystonia polypeptide 1 (DDP1/TIMM8/Tim8; (80)). Alternatively, defects in the MDRS/Mia40 pathway can lead to defects in mitofilin activity. Mitofilin is part of a large multisubunit protein complex in the mitochondrial inner membrane organizing system (MINOS) which controls cristae morphology, interacts with the TOM complex, promoting protein import into the intermembrane space via the MDRS/Mia40 pathway (76).

(ii) The majority of the mitochondrial outcomes exhibited a mutHtt gene–dose dependency, indicating that the higher number of mutated alleles is translated into a more severe outcome (Fig. 6) in both progenitors and neuron-like differentiated cells. Consistent with our studies, an accelerated rate of disease progression has also been reported in HM patients compared with HT (81) and in a knock-in mouse model of HD (82). However, a recent study showed that the age at onset of motor manifestations in HD is primarily determined by a single allelic dose of the mutant gene and not by the length of the normal allele, presence of a second mutant allele or absence of a normal allele. Although it is difficult to assess the contribution of 10 HM to that of >3000 HT patients, it is clear that biochemical parameters—such as those tested in this study—tend to be more sensitive (and present earlier onset) than motor skills.

(iii) The relatively late onset of HD features in patients or the progressive neurodegeneration may be explained by deficits in repair or clonal expansion of 'damaged' mtDNA which accumulates over time (based on replicative advantage of large-scale deletions (83)) outnumbering WT mtDNA (84). Thus, when reached a certain threshold becomes unsustainable and compensating mechanisms are no longer viable to delay the onset of aberrant outcomes.

Finally, elucidation of mechanisms relevant to mitochondrial function in HD is of critical relevance because it sets the background to develop targeted and rationale therapies that may delay the onset of symptoms.

## MATERIALS AND METHODS

### Chemicals and biochemicals

EDTA, EGTA, sodium succinate, mannitol, sucrose and HEPES were purchased from Sigma (St Louis, MO, USA). Tris–HCl, glycine, sodium chloride and KCl were purchased from Fisher (Pittsburg, PA, USA). Bovine serum albumin (fatty acid free) was obtained from MP Biomedicals. All reagents were of analytical grade.

### Cell culture conditions

Conditionally immortalized striatal neuronal progenitor cell lines were obtained either from the CHDI repository program. The STHdh$^{Q7/Q7}$ cell line expresses endogenous normal huntingtin, and the HT (STHdh$^{Q111/Q7}$) and HM (STHdh$^{Q111/Q111}$, previously described (85)) express mutant huntingtin with 111 Gln. The cells were plated in T75 flasks and grown at 33°C in a humidified atmosphere containing 5% $CO_2$ with 20 ml of Dulbecco's Modified Eagle Medium supplemented with 10% FBS (Hyclone #SH30071.03) and $10^4$ IU/ml penicillin and $10^4$ μg/ml streptomycin (Gibco). When at 80–90% confluence, the cells were plated in T75 flasks at a cell density of $2.5 \times 10^5$ per flask and selected in DMEM with 400 μg/ml G418 (Invitrogen). The cells were grown at 33°C for 3–5 days, changing the media every 2 to 3 days, until 80–90% confluent and then harvested by trypsinization, counted with a TC-10 cell counter (Bio-Rad) with 0.1% Trypan Blue, and used for the indicated analysis. Three T75 flasks for each condition were pooled for the measurements. When indicated, the cells were differentiated using a differentiation cocktail (10 ng/ml α-FGF, 250 μM 3--isobutyl-1-methylxanthine, 200 nM phorbol 12-myristate 13-acetate, 50 μM forskolin and 5 μM dopamine (85)).

### Evaluation of mitochondria mass and morphology by confocal microscopy

Cells (passages 11 and 12, $1 \times 10^5$) were seeded on sterile cover slips, grown over night at 33°C and then incubated for 30 min at 33°C with 0.5 μM MitoTracker Red CMXRos (MolecularProbes Inc., Eugene, OR, USA) diluted in growth media. After staining, cells were washed with media and fixed in 3.7% formaldehyde for 10 min. Fixed cells were then washed in PBS and blocked/permeabilized for 30 min in blocking buffer at room temperature, counterstained with 1 μg/ml 4′,6 diamidino-2-phenylindole (DAPI) and mounted on glass slides with anti-fading mounting media (Dako). Fluorescent images were obtained using an Olympus FV1000 laser scanning confocal microscope (excitation and emission wavelengths 594 and 660 nm) and analyzed with the Olympus Fluoview image analyzer with either a 20× or a 60× magnification.

For mitochondrial morphology quantification, approximately 20 cells for each cell line were analyzed using Image J to determine mitochondrial shape. Four distinct shapes were defined: miscellaneous, tubular, circular, and fragmented. These shapes were defined in Image J as follows: miscellaneous (Size: 50-Infinity, Circularity: 0–1), tubular (Size: 0–50, Circularity: 0–0.6); circular (Size: 0–50, Circularity: 0.6–1), fragmented (Size: 0–5, Circularity: 0–1). Using the sharpening feature within Image J, the various shapes were determined by shifting the threshold of the images (i.e. displaying only the pixels necessary for analysis while decreasing the image noise considerably). Then particle analysis, also a feature of Image J, was used to predict the shapes of these different shapes left in the image.

### Cell cycle analysis

FUCCI staining was performed according to manufacturer instructions (Invitrogen). This indicator employs a red (RFP) and a green (GFP) fluorescent protein fused to different regulators of the cell cycle, Cdt1 and geminin. In the G1 phase of the cell cycle, only Cdt1 tagged with RFP may be visualized, thus identifying cells in the G1 phase with red fluorescent nuclei. In the S, G2, and M phases, Cdt1 is degraded and only geminin-tagged with GFP remains, thus identifying cells in these phases with green fluorescent nuclei. During the G1/S transition both proteins are present in the cells, allowing GFP and RFP fluorescence to be observed—yellow fluorescence.

Progenitor HD cells (passages 11 and 12, $5 \times 10^4$) were plated onto polylysine coated coverslips and allowed to attach and grow overnight at 33°C. Incubation with the Premo™ FUCCI transduction solution was carried out after one cycle of cell doubling (in h, at 24, 28 and 33 after plating respectively for WT, HT and HM) at room temperature for 2 h, followed by incubation with BacMam enhancer for 60 min. Cells were fixed in 4% formaldehyde and imaged with an Olympus FV1000 laser scanning confocal microscope. Stained cells were counted and the results were expressed as percentage of the number of cells in each cell cycle phase (G1, G1/S and S/G2/M).

### Oxygen consumption measurements

The oxygen uptake of cell suspensions was measured using a Clark-type $O_2$ electrode from Hansatech (King's Lynn, UK) at 22°C. For oxygen uptake measurements of intact cells (passages 9 and 10), $1 \times 10^7$ cells/ml in complete growth media were supplemented with 5 μg/ml oligomycin, and the $O_2$ consumption was monitored for 2 min. Carbonyl cyanide 4-(trifluoromethoxy)phenylhydrazone (FCCP) (20 μM) was added to the medium and the oxygen consumption was recorded for additional 3–4 min. The rate of oxygen uptake with oligomycin was taken as State 4 oxygen uptake whereas that with FCCP as State 3u.

For oxygen consumption measurements cells were permeabilized as described previously (86). Briefly, attached cells were trypsinized and resuspended at a concentration of $1 \times 10^7$ in buffer A (10 mM $MgCl_2$, 20 mM HEPES, 250 mM sucrose, pH 7.4). Aliquots of cells were then treated with 2× recrystallized digitonin at a final concentration of 0.015% (which was found to be the optimal concentration in pilot studies) and mixed for 1 min. After centrifugation, the digitonin-containing buffer A was removed and permeabilized cells were washed with 5 volumes of buffer A to remove any remaining digitonin. During measurements, the chamber was thermostated at 22°C and sealed with a plunger. An electromagnetic stirrer bar was used to mix the contents of the chamber. Oxygen consumption rates were evaluated in buffer B (1 mM EGTA, 5 mM $MgCl_2$, 10 mM HEPES, 10 mM $KH_2PO_4$, 50 mM KCl, 220 mM sucrose, pH 7.4) in the presence of 1 mM malate-10 mM glutamate (NADH oxidase) followed by the addition of 5-μM rotenone and 10 mM succinate (succinate oxidase). Then, 10 mM malonate and 10 mM α-glycerophosphate were added to follow α-glycerophosphate oxidase rate. This rate was inhibited by adding 3.6 μM antimycin A.

### Complex activities and enzymatic assays

For enzymatic assays, an aliquot of the cells (passages 11–13) was spun down at 500 g for 5 min and resuspended (at a concentration of $5 \times 10^6$ cells/ml) in a hypotonic buffer (20 mM HEPES/KOH, pH 7.4) supplemented with phosphatase inhibitors (Sigma # P0044), and proteolytic inhibitors (Sigma # P2714), incubated on ice for 10–15 min, and homogenized with 30 strokes by a hand homogenizer, followed by two freeze-thawing cycles. Protein for the enzymatic assays was determined using the BCA assay kit from Pierce (Catalog #23227). Details on the methods used for each enzymatic assay were reported in the Supplementary Material, Supplementary Methods.

### Western blotting

Cells (passages 11 and 12, $1–2 \times 10^6$) were collected by trypsinization, pelleted by centrifugation at 300 × g for 5 min, extracted in RIPA buffer and then denaturated either in SDS-PAGE sample buffer (BioRad) plus 1.5% DTT at 100°C for 3 min or in NuPAGE sample buffer (Invitrogen)

plus 50 mM DTT at 70°C for 10 min. Details on the conditions used for electrophoresis, transfer and probing were reported in the Supplementary Material, Supplementary Methods. A description of the antibodies and conditions used is reported in Supplementary Material, Table S1.

### Total and mitochondrial ATP quantification

ATP levels were evaluated using a luciferase-based ATP determination kit (cat. No. A22066, Life Technology, Grand Island , NY, USA). WT, HT and HM cells (passages 11 and 12, $2 \times 10^5$) were plated in T75 flasks, grown for 48 h. Half of the cells for each cell line were then differentiated for 4 h as described. At the end of the differentiation process, one-third of the flasks (both progenitors and differentiated) were treated with 6 nM oligomycin (a specific inhibitor of mitochondrial Complex V), with the same volume of vehicle (DMSO) and no additions. After 90 min, the cells were collected by scraping, pelleted at 300*g* for 5 min and then suspended in deionized water (50–80 μl) and boiled at 100°C for 10 min to inactivate cellular ATPases. The resulting samples were then centrifuged again at 12 000*g* for 5 min and the supernatant was used to perform the ATP quantification assay according to the manufacturer's instructions. An ATP calibration curve was built between 0.01 and 0.5 μM. Luminescence values were recorded with a POLARstar Omega microplate reader (BMG Labtech, Cary, NC, USA). No differences in ATP concentrations were registered between vehicle-treated and untreated cells.

### Evaluation of mtDNA copy number and microdeletions

For evaluation of mtDNA copy number and deletions, quantitative real-time PCR (qT-PCR) with dual-labeled probes was performed. The targeted genes were the single-copy nuclear PK and mitochondrial ND1, ND4 and CYTB. Species-specific primers were selected using the Primer Express 3 software (Applied Biosystems). Mouse primers for PK were: forward 5′-CAGCCTCCCTGACGAGGTTAC-3′; reverse 5′-CTCCATCAACAAGCCGAAAAG-3′; the fluorogenic probe used was UPL 6 (Roche Universal Probe Library). ND1 primers were: forward 5′-CAAACACTTATTACAACCCAAGAACAC-3′; reverse 5′- AATCATATTATGGCTATGGGTCAGG-3′ and UPL 29 was used from Roche. ND4 primers were: forward 5′- ATCACTCCTATTCTGCCTAGCAAAC-3′; reverse 5′- AAGTCCTCGGGCCATGATTA-3′; Probe 5′-CCAACTACGAACGGATCCACAGCCGTA-3′. CYTB primers were: forward 5′-CCCAGACAACTACATACCAGC TAATC-3′; reverse 5′- AGGCTAGGACACCTCC TAGTTTATTG-3′; Probe 5′-TAAACACCCCACCCCATAT-TAAACCCGAA-3′. The corresponding real-time PCR efficiencies for each mitochondrial and nuclear gene amplification were calculated according to the equation: $E = 10^{(-1/\text{slope})} - 1$. After establishing the linear response between the Ct number and the template amount (25, 12.5, 6.25, 3.13 and 1.56 ng total per reaction), efficiencies for each gene were between 95 and 100%. Genomic DNA was extracted from cell cultures (P6–14) using a Puregene kit from Qiagen. DNA concentrations were determined by using Thermo Scientific's nanodrop. DNA was diluted to 0.626 ng/μl and served as a stock DNA template for qPCR. qPCR was performed in a Mastercycler EP Realplex thermocycler (Eppendorf, Westbury, NY, USA) with 7 μl of master mixture (TaqMan 2× PCR Master Mix; Applied Biosystems with 400 nM of primers and 80 nM of fluorogenic probes) and 5 μl of 3.13 ng total template were used per reaction. Amplification was performed using the default cycling parameters: 2 min at 50°C (activation of UNG enzyme), 95°C for 10 min (AmpliTaq Gold activation), followed by 40 cycles of 15 s of cycled denaturation at 95°C, 60 s annealing/extension at 60°C. The mean cycle time obtained by double derivatives (CalqPlex algorithm; Eppendorf) was designated as Ct. Relative mtDNA/nDNA was assessed by a comparative Ct method, using the following equation: $\text{mtDNA:nDNA} = 2^{-\Delta Ct}$, where $\Delta Ct = Ct_{\text{mitochondrial}} - Ct_{\text{nuclear}}$. Each sample was analyzed in triplicates. Positive and negative controls were run in each plate.

### Evaluation of hydrogen peroxide concentrations in cells in culture

Hydrogen peroxide ($H_2O_2$) was measured using the Amplex red hydrogen peroxide assay kit (Life Technologies, NY, USA). Cells (passages 11 and 12, 2 × T75 flasks for each cell line at a density of $4 \times 10^5$) were grown in regular growth media for 24 h. The cells were then collected by trypsinization and counted with a TC10 cell counter (Bio-Rad). The $H_2O_2$ quantification assay was carried out in a 96-well plate with $0.2–0.5 \times 10^5$ progenitor or differentiated striatal cells in a final volume of 100 μl of growth media (without phenol red) in the presence of horseradish peroxidase (0.2 U/ml) and Amplex red reagent (100 μM). The oxidized product or resorufin, produced in a 1 $H_2O_2$: 1 product stoichiometry, exhibits a maximum absorbance at 560 nm. The production of $H_2O_2$ was followed for 30 min at 37°C and 560 nm in an infinite spectrophotometer and expressed as nmol $H_2O_2$ produced × $(\text{h} \times 10^6 \text{ cells})^{-1}$.

### Statistical and power analyses

The number of experiments per group required to reach statistical significance (with alpha and beta fixed at 0.05 and 0.95) was computed using G*power analysis from an *a priori* analysis. Experiments were run in triplicates and repeated three times in independent experiments unless noted otherwise. Data were expressed as mean ± standard error. The data were evaluated by the analysis of variance (ANOVA) followed by Bonferroni's post-test using GraphPad Prism (GraphPad Software Incorporation, La Jolla, CA, USA) and considering $P \leq 0.05$ as statistically significant unless indicated.

## SUPPLEMENTARY MATERIAL

Supplementary Material is available at *HMG* online.

## ACKNOWLEDGEMENTS

We thank the technical assistance of Ms Alicja Omanska-Klusek, Mr. Billy Zhang, and Dr Robert Schoenfeld. We are

grateful to Dr Marcie McDonald (Harvard University) for donating the cell lines at early passages.

*Conflict of Interest statement*: None declared.

## FUNDING

This study was funded by CHDI (A-2638) to C.G.

## REFERENCES

1. Martin, J.B. and Gusella, J.F. (1986) Huntington's disease. Pathogenesis and management. *N. Engl. J. Med.*, **315**, 1267–1276.
2. Vonsattel, J.P., Myers, R.H., Stevens, T.J., Ferrante, R.J., Bird, E.D. and Richardson, E.P. Jr. (1985) Neuropathological classification of Huntington's disease. *J. Neuropathol. Exp. Neurol.*, **44**, 559–577.
3. Folstein, S.E., Leigh, R.J., Parhad, I.M. and Folstein, M.F. (1986) The diagnosis of Huntington's disease. *Neurology*, **36**, 1279–1283.
4. Craufurd, D., Thompson, J.C. and Snowden, J.S. (2001) Behavioral changes in Huntington disease. *Neuropsychiatry Neuropsychol. Behav. Neurol.*, **14**, 219–226.
5. MacDonald, M.E., Ambrose, C.M., Duyao, M.P., Myers, R.H., Lin, C., Srinidhi, L., Barnes, G., Taylor, S.A., James, M., Groot, N. *et al.* (1993) A novel gene containing a trinucleotide repeat that is expanded and unstable on Huntington's disease chromosomes. *Cell*, **72**, 971–983.
6. Snell, R.G., MacMillan, J.C., Cheadle, J.P., Fenton, I., Lazarou, L.P., Davies, P., MacDonald, M.E., Gusella, J.F., Harper, P.S. and Shaw, D.J. (1993) Relationship between trinucleotide repeat expansion and phenotypic variation in Huntington's disease. *Nat. Genet.*, **4**, 393–397.
7. Sapp, E., Penney, J., Young, A., Aronin, N., Vonsattel, J.P. and DiFiglia, M. (1999) Axonal transport of N-terminal huntingtin suggests early pathology of corticostriatal projections in Huntington disease. *J. Neuropathol. Exp. Neurol.*, **58**, 165–173.
8. Li, H., Li, S.H., Johnston, H., Shelbourne, P.F. and Li, X.J. (2000) Amino-terminal fragments of mutant huntingtin show selective accumulation in striatal neurons and synaptic toxicity. *Nat. Genet.*, **25**, 385–389.
9. Turner, C. and Schapira, A.H. (2010) Mitochondrial matters of the brain: the role in Huntington's disease. *J. Bioenerg. Biomembr.*, **42**, 193–198.
10. Kuhl, D.E., Markham, C.H., Metter, E.J., Riege, W.H., Phelps, M.E. and Mazziotta, J.C. (1985) Local cerebral glucose utilization in symptomatic and presymptomatic Huntington's disease. *Res. Publ. Assoc. Res. Nerv. Ment. Dis.*, **63**, 199–209.
11. Kuhl, D.E., Metter, E.J., Riege, W.H. and Markham, C.H. (1984) Patterns of cerebral glucose utilization in Parkinson's disease and Huntington's disease. *Ann. Neurol.*, **15**(Suppl), S119–S125.
12. Kuhl, D.E., Phelps, M.E., Markham, C.H., Metter, E.J., Riege, W.H. and Winter, J. (1982) Cerebral metabolism and atrophy in Huntington's disease determined by 18FDG and computed tomographic scan. *Ann. Neurol.*, **12**, 425–434.
13. Feigin, A., Leenders, K.L., Moeller, J.R., Missimer, J., Kuenig, G., Spetsieris, P., Antonini, A. and Eidelberg, D. (2001) Metabolic network abnormalities in early Huntington's disease: an [18F]FDG PET study. *J. Nucl. Med.*, **42**, 1591–1595.
14. Browne, S.E. and Beal, M.F. (2004) The energetics of Huntington's disease. *Neurochem. Res.*, **29**, 531–546.
15. Browne, S.E., Bowling, A.C., MacGarvey, U., Baik, M.J., Berger, S.C., Muqit, M.M., Bird, E.D. and Beal, M.F. (1997) Oxidative damage and metabolic dysfunction in Huntington's disease: selective vulnerability of the basal ganglia. *Ann. Neurol.*, **41**, 646–653.
16. Gu, M., Gash, M.T., Mann, V.M., Javoy-Agid, F., Cooper, J.M. and Schapira, A.H. (1996) Mitochondrial defect in Huntington's disease caudate nucleus. *Ann. Neurol.*, **39**, 385–389.
17. Mann, V.M., Cooper, J.M., Javoy-Agid, F., Agid, Y., Jenner, P. and Schapira, A.H. (1990) Mitochondrial function and parental sex effect in Huntington's disease. *Lancet*, **336**, 749.
18. Milakovic, T. and Johnson, G.V. (2005) Mitochondrial respiration and ATP production are significantly impaired in striatal cells expressing mutant huntingtin. *J. Biol. Chem.*, **280**, 30773–30782.
19. Guidetti, P., Charles, V., Chen, E.Y., Reddy, P.H., Kordower, J.H., Whetsell, W.O., Schwarcz, R. and Tagle, D.A. (2001) Early degenerative changes in transgenic mice expressing mutant huntingtin involve dendritic abnormalities but no impairment of mitochondrial energy production. *Exp. Neurol.*, **169**, 340–350.
20. Higgins, D.S., Hoyt, K.R., Baic, C., Vensel, J. and Sulka, M. (1999) Metabolic and glutamatergic disturbances in the Huntington's disease transgenic mouse. *Ann. N. Y. Acad. Sci.*, **893**, 298–300.
21. Bae, B.I., Xu, H., Igarashi, S., Fujimuro, M., Agrawal, N., Taya, Y., Hayward, S.D., Moran, T.H., Montell, C., Ross, C.A. *et al.* (2005) p53 mediates cellular dysfunction and behavioral abnormalities in Huntington's disease. *Neuron*, **47**, 29–41.
22. Tabrizi, S.J., Workman, J., Hart, P.E., Mangiarini, L., Mahal, A., Bates, G., Cooper, J.M. and Schapira, A.H. (2000) Mitochondrial dysfunction and free radical damage in the Huntington R6/2 transgenic mouse. *Ann. Neurol.*, **47**, 80–86.
23. Brustovetsky, N., LaFrance, R., Purl, K.J., Brustovetsky, T., Keene, C.D., Low, W.C. and Dubinsky, J.M. (2005) Age-dependent changes in the calcium sensitivity of striatal mitochondria in mouse models of Huntington's disease. *J. Neurochem.*, **93**, 1361–1370.
24. Brustovetsky, N., Brustovetsky, T., Purl, K.J., Capano, M., Crompton, M. and Dubinsky, J.M. (2003) Increased susceptibility of striatal mitochondria to calcium-induced permeability transition. *J. Neurosci.*, **23**, 4858–4867.
25. Choo, Y.S., Johnson, G.V., MacDonald, M., Detloff, P.J. and Lesort, M. (2004) Mutant huntingtin directly increases susceptibility of mitochondria to the calcium-induced permeability transition and cytochrome c release. *Hum. Mol. Genet.*, **13**, 1407–1420.
26. Panov, A.V., Gutekunst, C.A., Leavitt, B.R., Hayden, M.R., Burke, J.R., Strittmatter, W.J. and Greenamyre, J.T. (2002) Early mitochondrial calcium defects in Huntington's disease are a direct effect of polyglutamines. *Nat. Neurosci.*, **5**, 731–736.
27. Fukui, H. and Moraes, C.T. (2007) Extended polyglutamine repeats trigger a feedback loop involving the mitochondrial complex III, the proteasome and huntingtin aggregates. *Hum. Mol. Genet.*, **16**, 783–797.
28. Chaturvedi, R.K., Adhihetty, P., Shukla, S., Hennessy, T., Calingasan, N., Yang, L., Starkov, A., Kiaei, M., Cannella, M., Sassone, J. *et al.* (2009) Impaired PGC-1alpha function in muscle in Huntington's disease. *Hum. Mol. Genet.*, **18**, 3048–3065.
29. DiMauro, S. and Schon, E.A. (2008) Mitochondrial disorders in the nervous system. *Annu. Rev. Neurosci.*, **31**, 91–123.
30. Mesecke, N., Terziyska, N., Kozany, C., Baumann, F., Neupert, W., Hell, K. and Herrmann, J.M. (2005) A disulfide relay system in the intermembrane space of mitochondria that mediates protein import. *Cell*, **121**, 1059–1069.
31. Farrell, S.R. and Thorpe, C. (2005) Augmenter of liver regeneration: a flavin-dependent sulfhydryl oxidase with cytochrome c reductase activity. *Biochemistry*, **44**, 1532–1541.
32. Hell, K. (2008) The Erv1-Mia40 disulfide relay system in the intermembrane space of mitochondria. *Biochim. Biophys. Acta*, **1783**, 601–609.
33. Lu, H., Allen, S., Wardleworth, L., Savory, P. and Tokatlidis, K. (2004) Functional TIM10 chaperone assembly is redox-regulated in vivo. *J. Biol. Chem.*, **279**, 18952–18958.
34. Lutz, T., Neupert, W. and Herrmann, J.M. (2003) Import of small tim proteins into the mitochondrial intermembrane space. *EMBO J.*, **22**, 4400–4408.
35. Lange, H., Lisowsky, T., Gerber, J., Muhlenhoff, U., Kispal, G. and Lill, R. (2001) An essential function of the mitochondrial sulfhydryl oxidase Erv1p/ALR in the maturation of cytosolic Fe/S proteins. *EMBO Rep.*, **2**, 715–720.
36. Lisowsky, T. (1992) Dual function of a new nuclear gene for oxidative phosphorylation and vegetative growth in yeast. *Mol. Gen. Genet.*, **232**, 58–64.
37. Lisowsky, T. (1994) ERV1 is involved in the cell-division cycle and the maintenance of mitochondrial genomes in Saccharomyces cerevisiae. *Curr. Genet.*, **26**, 15–20.
38. Becher, D., Kricke, J., Stein, G. and Lisowsky, T. (1999) A mutant for the yeast scERV1 gene displays a new defect in mitochondrial morphology and distribution. *Yeast*, **15**, 1171–1181.
39. Di Fonzo, A., Ronchi, D., Lodi, T., Fassone, E., Tigano, M., Lamperti, C., Corti, S., Bordoni, A., Fortunato, F., Nizzardo, M. *et al.* (2009) The mitochondrial disulfide relay system protein GFER is mutated in autosomal-recessive myopathy with cataract and combined respiratory-chain deficiency. *Am. J. Hum. Genet.*, **84**, 594–604.

40. Sideris, D.P., Petrakis, N., Katrakili, N., Mikropoulou, D., Gallo, A., Ciofi-Baffoni, S., Banci, L., Bertini, I. and Tokatlidis, K. (2009) A novel intermembrane space-targeting signal docks cysteines onto Mia40 during mitochondrial oxidative folding. *J. Cell. Biol.*, **187**, 1007–1022.
41. Angerer, H., Zwicker, K., Wumaier, Z., Sokolova, L., Heide, H., Steger, M., Kaiser, S., Nubel, E., Brutschy, B., Radermacher, M. *et al.* (2011) A scaffold of accessory subunits links the peripheral arm and the distal proton-pumping module of mitochondrial complex I. *Biochem. J.*, **437**, 279–288.
42. Cavallaro, G. (2010) Genome-wide analysis of eukaryotic twin CX9C proteins. *Mol. Biosyst.*, **6**, 2459–2470.
43. Antonicka, H., Ogilvie, I., Taivassalo, T., Anitori, R.P., Haller, R.G., Vissing, J., Kennaway, N.G. and Shoubridge, E.A. (2003) Identification and characterization of a common set of complex I assembly intermediates in mitochondria from patients with complex I deficiency. *J. Biol. Chem.*, **278**, 43081–43088.
44. Vogel, R.O., Dieteren, C.E., van den Heuvel, L.P., Willems, P.H., Smeitink, J.A., Koopman, W.J. and Nijtmans, L.G. (2007) Identification of mitochondrial complex I assembly intermediates by tracing tagged NDUFS3 demonstrates the entry point of mitochondrial subunits. *J. Biol. Chem.*, **282**, 7582–7590.
45. Grivennikova, V.G., Kapustin, A.N. and Vinogradov, A.D. (2001) Catalytic activity of NADH-ubiquinone oxidoreductase (complex I) in intact mitochondria. Evidence for the slow active/inactive transition. *J. Biol. Chem.*, **276**, 9038–9044.
46. Papa, S. (2002) The NDUFS4 nuclear gene of complex I of mitochondria and the cAMP cascade. *Biochim. Biophys. Acta*, **1555**, 147–153.
47. Elpeleg, O. (2003) Inherited mitochondrial DNA depletion. *Pediatr. Res.*, **54**, 153–159.
48. Rotig, A. and Poulton, J. (2009) Genetic causes of mitochondrial DNA depletion in humans. *Biochim. Biophys. Acta*, **1792**, 1103–1108.
49. Cantatore, P., Daddabbo, L., Fracasso, F. and Gadaleta, M.N. (1995) Identification by in organello footprinting of protein contact sites and of single-stranded DNA sequences in the regulatory region of rat mitochondrial DNA. Protein binding sites and single-stranded DNA regions in isolated rat liver mitochondria. *J. Biol. Chem.*, **270**, 25020–25027.
50. Martherus, R.S.R.M., Sluiter, W., Timmer, E.D.J., Van, H.S.J.V., Smeets, H.J.M. and Ayoubi, T.A.Y. (2010) Functional annotation of heart enriched mitochondrial genes GBAS and CHCHD10 through guilt by association. *Biochem. Biophys. Res. Commun.*, **402**, 203–208.
51. Darshi, M., Mendiola, V.L., Mackey, M.R., Murphy, A.N., Koller, A., Perkins, G.A., Ellisman, M.H. and Taylor, S.S. (2011) ChChd3, an inner mitochondrial membrane protein, is essential for maintaining crista integrity and mitochondrial function. *J. Biol. Chem.*, **286**, 2918–2932.
52. Muller, M. and Reichert, A.S. (2011) Mitophagy, mitochondrial dynamics and the general stress response in yeast. *Biochem. Soc. Trans.*, **39**, 1514–1519.
53. Narendra, D.P., Jin, S.M., Tanaka, A., Suen, D.F., Gautier, C.A., Shen, J., Cookson, M.R. and Youle, R.J. (2010) PINK1 is selectively stabilized on impaired mitochondria to activate Parkin. *PLoS Biol.*, **8**, e1000298.
54. West, A.B., Moore, D.J., Biskup, S., Bugayenko, A., Smith, W.W., Ross, C.A., Dawson, V.L. and Dawson, T.M. (2005) Parkinson's disease-associated mutations in leucine-rich repeat kinase 2 augment kinase activity. *Proc. Natl Acad. Sci. USA*, **102**, 16842–16847.
55. Xu, E.H., Tang, Y., Li, D. and Jia, J.P. (2009) Polymorphism of HD and UCHL-1 genes in Huntington's disease. *J. Clin. Neurosci.*, **16**, 1473–1477.
56. Poot, M., Zhang, Y.Z., Kramer, J.A., Wells, K.S., Jones, L.J., Hanzel, D.K., Lugade, A.G., Singer, V.L. and Haugland, R.P. (1996) Analysis of mitochondrial morphology and function with novel fixable fluorescent stains. *J. Histochem. Cytochem.*, **44**, 1363–1372.
57. Liot, G., Bossy, B., Lubitz, S., Kushnareva, Y., Sejbuk, N. and Bossy-Wetzel, E. (2009) Complex II inhibition by 3-NP causes mitochondrial fragmentation and neuronal cell death via an NMDA- and ROS-dependent pathway. *Cell Death Differ.*, **16**, 899–909.
58. Song, W., Chen, J., Petrilli, A., Liot, G., Klinglmayr, E., Zhou, Y., Poquiz, P., Tjong, J., Pouladi, M.A., Hayden, M.R. *et al.* (2011) Mutant huntingtin binds the mitochondrial fission GTPase dynamin-related protein-1 and increases its enzymatic activity. *Nat. Med.*, **17**, 377–382.
59. Rossignol, R., Letellier, T., Malgat, M., Rocher, C. and Mazat, J.P. (2000) Tissue variation in the control of oxidative phosphorylation: implication for mitochondrial diseases. *Biochem. J.*, **347**(Pt 1), 45–53.
60. Galkin, A. and Moncada, S. (2007) S-nitrosation of mitochondrial complex I depends on its structural conformation. *J. Biol. Chem.*, **282**, 37448–37453.
61. Saulle, E., Gubellini, P., Picconi, B., Centonze, D., Tropepi, D., Pisani, A., Morari, M., Marti, M., Rossi, L., Papa, M. *et al.* (2004) Neuronal vulnerability following inhibition of mitochondrial complex II: a possible ionic mechanism for Huntington's disease. *Mol. Cell Neurosci.*, **25**, 9–20.
62. Shirendeb, U.P., Calkins, M.J., Manczak, M., Anekonda, V., Dufour, B., McBride, J.L., Mao, P. and Reddy, P.H. (2012) Mutant huntingtin's interaction with mitochondrial protein Drp1 impairs mitochondrial biogenesis and causes defective axonal transport and synaptic degeneration in Huntington's disease. *Hum. Mol. Genet.*, **21**, 406–420.
63. Sirrenberg, C., Endres, M., Becker, K., Bauer, M.F., Walther, E., Neupert, W. and Brunner, M. (1997) Functional cooperation and stoichiometry of protein translocases of the outer and inner membranes of mitochondria. *J. Biol. Chem.*, **272**, 29963–29966.
64. Tchakarska, G., Roussel, M., Troussard, X. and Sola, B. (2011) Cyclin D1 inhibits mitochondrial activity in B cells. *Cancer Res.*, **71**, 1690–1699.
65. Campanella, M., Parker, N., Tan, C.H., Hall, A.M. and Duchen, M.R. (2009) IF1: setting the pace of the F1Fo-ATP synthase. *Trends Biochem. Sci.*, **34**, 343–350.
66. Faccenda, D. and Campanella, M. (2012) Molecular regulation of the mitochondrial F(1)F(o)-ATPsynthase: physiological and pathological significance of the inhibitory factor 1 (IF(1)). *Int. J. Cell. Biol.*, **2012**, 367934.
67. Cabezon, E., Arechaga, I., Jonathan, P., Butler, G. and Walker, J.E. (2000) Dimerization of bovine F1-ATPase by binding the inhibitor protein, IF1. *J. Biol. Chem.*, **275**, 28353–28355.
68. Fujisawa, Y., Kato, K. and Giulivi, C. (2009) Nitration of tyrosine residues 368 and 345 in the beta-subunit elicits F0F1-ATPase activity loss. *Biochem. J.*, **423**, 219–231.
69. Bence, N.F., Sampat, R.M. and Kopito, R.R. (2001) Impairment of the ubiquitin-proteasome system by protein aggregation. *Science*, **292**, 1552–1555.
70. Hou, X., Liu, J.E., Liu, W., Liu, C.Y., Liu, Z.Y. and Sun, Z.Y. (2011) A new role of NUAK1: directly phosphorylating p53 and regulating cell proliferation. *Oncogene*, **30**, 2933–2942.
71. Jones, R.G., Plas, D.R., Kubek, S., Buzzai, M., Mu, J., Xu, Y., Birnbaum, M.J. and Thompson, C.B. (2005) AMP-activated protein kinase induces a p53-dependent metabolic checkpoint. *Mol. Cell.*, **18**, 283–293.
72. Parker, W.D. Jr., Boyson, S.J., Luder, A.S. and Parks, J.K. (1990) Evidence for a defect in NADH: ubiquinone oxidoreductase (complex I) in Huntington's disease. *Neurology*, **40**, 1231–1234.
73. Arenas, J., Campos, Y., Ribacoba, R., Martin, M.A., Rubio, J.C., Ablanedo, P. and Cabello, A. (1998) Complex I defect in muscle from patients with Huntington's disease. *Ann. Neurol.*, **43**, 397–400.
74. Siddiqui, A., Rivera-Sanchez, S., Castro Mdel, R., Acevedo-Torres, K., Rane, A., Torres-Ramos, C.A., Nicholls, D.G., Andersen, J.K. and Ayala-Torres, S. (2012) Mitochondrial DNA damage Is associated with reduced mitochondrial bioenergetics in Huntington's disease. *Free Radic. Biol. Med.*, **53**, 1478–1488.
75. Gomes, L.C., Di Benedetto, G. and Scorrano, L. (2011) During autophagy mitochondria elongate, are spared from degradation and sustain cell viability. *Nat. Cell Biol.*, **13**, 589–598.
76. Stojanovski, D., Bohnert, M., Pfanner, N. and van der Laan, M. (2012) Mechanisms of protein sorting in mitochondria. *Cold Spring Harb. Perspect. Biol.*, **4**, 1–18.
77. Bauer, M.F., Hofmann, S., Neupert, W. and Brunner, M. (2000) Protein translocation into mitochondria: the role of TIM complexes. *Trends Cell Biol.*, **10**, 25–31.
78. Kerscher, O., Holder, J., Srinivasan, M., Leung, R.S. and Jensen, R.E. (1997) The Tim54p-Tim22p complex mediates insertion of proteins into the mitochondrial inner membrane. *J. Cell Biol.*, **139**, 1663–1675.
79. Chacinska, A., Lind, M., Frazier, A.E., Dudek, J., Meisinger, C., Geissler, A., Sickmann, A., Meyer, H.E., Truscott, K.N., Guiard, B. *et al.* (2005) Mitochondrial presequence translocase: switching between TOM tethering and motor recruitment involves Tim21 and Tim17. *Cell*, **120**, 817–829.
80. Koehler, C.M., Leuenberger, D., Merchant, S., Renold, A., Junne, T. and Schatz, G. (1999) Human deafness dystonia syndrome is a mitochondrial disease. *Proc. Natl Acad. Sci. USA*, **96**, 2141–2146.

81. Squitieri, F., Gellera, C., Cannella, M., Mariotti, C., Cislaghi, G., Rubinsztein, D.C., Almqvist, E.W., Turner, D., Bachoud-Levi, A.C., Simpson, S.A. *et al.* (2003) Homozygosity for CAG mutation in Huntington disease is associated with a more severe clinical course. *Brain*, **126**, 946–955.
82. Lin, C.H., Tallaksen-Greene, S., Chien, W.M., Cearley, J.A., Jackson, W.S., Crouse, A.B., Ren, S., Li, X.J., Albin, R.L. and Detloff, P.J. (2001) Neurological abnormalities in a knock-in mouse model of Huntington's disease. *Hum. Mol. Genet.*, **10**, 137–144.
83. Tang, Y., Manfredi, G., Hirano, M. and Schon, E.A. (2000) Maintenance of human rearranged mitochondrial DNAs in long-term cultured transmitochondrial cell lines. *Mol. Biol. Cell.*, **11**, 2349–2358.
84. Yoneda, M., Chomyn, A., Martinuzzi, A., Hurko, O. and Attardi, G. (1992) Marked replicative advantage of human mtDNA carrying a point mutation that causes the MELAS encephalomyopathy. *Proc. Natl Acad. Sci. USA*, **89**, 11164–11168.
85. Trettel, F., Rigamonti, D., Hilditch-Maguire, P., Wheeler, V.C., Sharp, A.H., Persichetti, F., Cattaneo, E. and MacDonald, M.E. (2000) Dominant phenotypes produced by the HD mutation in STHdhQ111 striatal cells. *Hum. Mol. Genet.*, **9**, 2799–2809.
86. Hofhaus, G., Shakeley, R.M. and Attardi, G. (1996) [41] Use of polarography to detect respiration defects in cell cultures. *Methods Enzymol.*, **264**, 476–480.